Electrochimica Acta 56 (2011) 5561–5565

Contents lists available at ScienceDirect

Electrochimica Acta

journal homepage: www.elsevier.com/locate/electacta

Synthesis and magneto-transport properties of single PEDOT/Ni and PEDOT/$Ni_{30}Fe_{70}$ core/shell nanowires

Carlos M. Hangarter[a], Youngwoo Rheem[a], Thomas Stahovich[b], Nosang V. Myung[a,*]

[a] Chemical & Environmental Engineering and Center for Nanoscale Science and Engineering, University of California-Riverside, Riverside, CA 92521, United States
[b] Mechanical Engineering, University of California-Riverside, Riverside, CA 92521, United States

ARTICLE INFO

Article history:
Received 12 May 2010
Received in revised form 17 March 2011
Accepted 21 March 2011
Available online 2 April 2011

Keywords:
Ferromagnetic
PEDOT nanowire
Positive templated electrodeposition
Magnetoresistance
Core/shell
Domain wall magnetoresistance

ABSTRACT

Single polyethylenedioxythiophene (PEDOT) nanowires bridging pairs of electrodes were utilized as positive templates to create PEDOT/Ni and PEDOT/$Ni_{30}Fe_{70}$ core/shell nanowires by electrodepositing ferromagnetic material (i.e., Ni and $Ni_{30}Fe_{70}$) on the entire assembly, including both the electrodes and nanowire. The temperature dependence of the electrical resistance indicated that electrons are transported predominately through the ferromagnetic shell. The magnetoresistive (MR) behavior of the core/shell nanowires was investigated as a function of temperature, magnetic field orientation, shell thickness, and composition. The MR behavior of the PEDOT/Ni core/shell nanowires was anomalous for low applied magnetic fields, deviating from expected anisotropic magnetoresistance, with positive $\Delta R/R_O$ values for all field orientations. PEDOT/$Ni_{30}Fe_{70}$ core/shell nanowires displayed the opposite behavior, with negative $\Delta R/R_O$ for both longitudinal and transverse field orientations. The origin of this magnetoresistive behavior is postulated to be a geometry induced domain wall effect.

1. Introduction

Ferromagnetic nanotubes have attracted attention as potential candidates for magnetic recording media, read/write heads [1], drug delivery/bioseparation constituents [2,3], sensors, and optoelectronic devices [4–7]. The cavity of a nanotube, with its radial interfaces, presents a means to complement the inherent magnetism with additional functionality. For example, ferromagnetic shell coatings over conducting polymer nanotubes have been demonstrated to significantly enhance photoluminescence efficiency of polymer nanotubes due to charge transfer from surface plasmon resonance coupling [4,5]. In addition, significant effort has also been made to characterize the magnetization state and reversal modes of ferromagnetic nanotubes, which have been found to be largely dependent on the ratio of inner to outer radius, and the ratio of outer radius to length [8–11]. These studies have found that the nanotube yields a magnetic configuration that eliminates a mathematical singularity found in wires, enabling faster and more reproducible switching for data storage applications [9,12]. To synthesize ferromagnetic nanotubes, a variety of nanoporous template-assisted methods have been used, including electrodeposition [13,14], electroless deposition [15], hydrogen reduction [13,16,17], atomic layer deposition [18,19], Kirkendall diffusion [20], core etching [21], and nanoparticle assembly [22]. Investigators have studied a variety of magnetic properties of these structures, such as coercivity, remanance, and squareness. However, there has been significantly less work aimed at understanding the magneto-transport properties of ferromagnetic nanotubes.

Magnetoresistance (MR), which is important for magnetic sensors, magnetic random access memory (MRAM), and data storage applications, can be broadly defined as a change in the electrical resistance in response to a applied magnetic field. Several different phenomena can cause this behavior. For example, interfacial spin accumulation can generate giant magnetoresistance (GMR), s-d scattering of electrons can produce anisotropic magnetoresistance (AMR), and spin dependent tunneling of electrons across an insulating barrier can cause tunneling magnetoresistance (TMR). Geometry-induced MR behavior has been studied much less extensively than physical MR mechanisms, but has significant promise for MR signal enhancement [23,24]. Structures producing geometry-induced MR typically have concentric surfaces and rely on geometric disruption of magneto-transport vector quantities to enhance the response to imposed magnetic fields. Techniques to miniaturize geometry-based MR devices are important to the design and development of magnetic sensors, components of position/motion detectors, and an emerging class of biosensors.

Here a facile technique for synthesizing individual conducting polymer/ferromagnetic core/shell nanowires is reported. This approach utilizes laterally aligned PEDOT nanowires as positive templates for electrodepositing ferromagnetic shells, which can then be characterized in terms of magneto-transport properties.

* Corresponding author. Tel.: +1 951 827 7710; fax: +1 951 827 5696.
E-mail address: myung@engr.ucr.edu (N.V. Myung).

0013-4686/$ – see front matter © 2011 Elsevier Ltd. All rights reserved.
doi:10.1016/j.electacta.2011.03.115

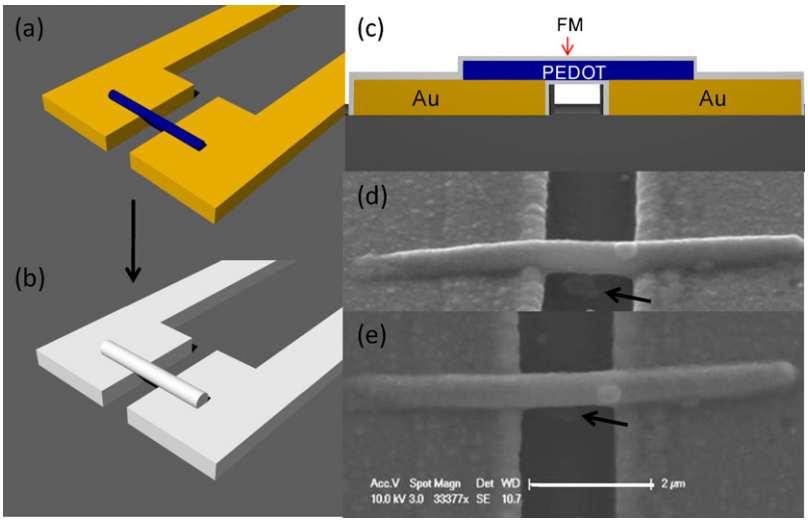

Fig. 1. Schematic of PEDOT/ferromagnetic core/shell nanowire device fabrication starting with (a) a single PEDOT nanowire bridging prefabricated microelectrodes followed by (b) electrodeposition of the ferromagnetic material over the entire assembly. (c) All the components of the completed device, including Au or Ni electrodes, PEDOT nanowire, and FM coating, are illustrated and labeled in the schematic cross-section. SEM images of a PEDOT/$Ni_{30}Fe_{70}$ core/shell nanowire are shown from two different perspectives: (d) 45° tilt and (e) top-view. Arrows indicate residue underneath core/shell nanowire for angle perspective. Scale bars represents 2 μm.

In contrast to nanoporous template methodologies, this in situ fabrication process eliminates post-synthesis assembly operations, which can be difficult due to the inherent fragility of the structures. It also avoids the formation of native oxide layer contact barriers that readily form on these high-surface-area iron-group nanostructures [25,26]. Another advantage of the in situ process is that it results in solid and rigid electrical contacts, avoiding aberrant results from series contact resistance.

To verify that electrical transport occurs predominately through the ferromagnetic shell, these devices were characterized in terms of the temperature coefficient of resistance (TCR). The MR behavior was examined as a function of temperature and magnetic field orientation for both Ni and $Ni_{30}Fe_{70}$ shells. The influence of wall thicknesses on magneto-transport properties was studied only for the PEDOT/Ni core/shell nanowires. Analysis of these results provides evidence for the existence of geometry-induced magnetoresistance, which is fundamentally different than the AMR behavior typically observed for Ni.

2. Experimental

PEDOT nanowires were synthesized using an anodic aluminum oxide membrane (Whatman Anodisc 13) with a gold seed layer serving as the cathode. The PEDOT nanowires were electropolymerized from an aqueous bath of 50 mM 3,4-ethylendioxythiophene, 100 mM $LiClO_4$, and 100 mM sodium dodecyl sulfate, with an applied potential of 1.0 V vs. a saturated calomel electrode (SCE). Pt was used as a counter electrode. The solution was purged with high purity Argon (99.99%) for 30 min prior to use to minimize the oxidation of monomers. Anodic electrodeposition of PEDOT nanowires was performed at room temperature with agitation from a 1″ stirbar at 300 rpm in a cell covered with aluminum foil to mitigate photo-polymerization. The dopants, ClO_4^- and dodecyl sulfate (DS), were selected to provide high conductivity and low dopant mobility, respectively. Embedded nanowires were removed by polishing the seed layer and etching the template in 30% H_3PO_4 (v/v).

Single PEDOT nanowire devices were fabricated with AC dielectrophoretic assembly of a PEDOT nanowire on prefabricated electrodes. Different electrode shapes, including square, rectangular and centered fingers, and various electrode materials, including Au and Ni, were also investigated to discount their possible influence in these measurements. Alignment conditions were optimized for PEDOT nanowires with both Au and Ni electrodes with a peak to peak potential of 1 V and 0.5 V, respectively. Aqueous suspensions were used for the Au electrodes, while isopropanol was used to prevent dissolution of the Ni electrodes. After dispensing 10 μl of nanowire suspension on either the Au or Ni electrodes, a sinusoidal waveform was applied for approximately 10 s at 5 MHz. After alignment, aqueous droplets were removed with N_2 and isopropanol was allowed to evaporate. The alignment times were adjusted according to the nanowire suspension concentration, which was on the order of 10^9 ml^{-1}. Nanowire assembly procedures were repeated until a single bridging nanowire was formed. Bridging nanowires were confirmed using a Hirox KH3000 optical microscope.

To electrodeposit ferromagnetic shells on the PEDOT nanowires, the electrodes were shorted to each other to form a single electrical lead. The working areas for centered finger, square, and rectangular electrodes were 0.023, 0.043, and 0.072 cm^2, respectively. The nanowire/electrode assemblies were subsequently electroplated with either Ni or $Ni_{30}Fe_{70}$. The Ni bath consisted of 1.5 M $Ni(SO_3NH_2)_2$, 0.2 M $NiCl_2$, and 0.4 M H_3BO_3 at a pH of 4.0. Ni shells were electrodeposited at a deposition potential of −1.1 V vs. saturated calomel electrode (SCE) at room temperature with no agitation for short time periods (10–30 s). $Ni_{30}Fe_{70}$ shells were electrodeposited using a two-electrode configuration with a Pt mesh counter electrode. The electrolyte consisted of 0.2 M $NiCl_2$, 0.06 M $FeCl_2$, 0.05 M L'ascorbic acid, 0.0075 M saccharin, 0.7 M NaCl, and 0.4 M H_3BO_3. This bath was agitated with a 1″ stirbar at 300 rpm under ambient conditions with an applied current density of −5 mA/cm^2 for 2 min. L'ascorbic acid was added to prevent Fe^{2+} oxidation, saccharin was added as a stress reliever, and H_3BO_3 was added as a pH buffer.

The magneto-transport properties of individual core/shell nanowires were measured at temperatures from 10 to 300 K using a physical property measurement system by Quantum Design. The effect of magnetic-field orientation on MR behavior was measured in 15° increments with the magnetic field alignment ranging from a longitudinal (0°) to a transverse (90°) orientation with respect to the electric field/nanowire axis. The TCR was extracted from temperature dependent MR measurements. The morphology of core/shell nanowires was imaged with a Phillips XL30-FEG scanning electron microscope (SEM).

3. Results and discussion

The fabrication process for single conducting polymer/ferromagnetic core/shell nanowires is shown schematically in Fig. 1. To start, a single PEDOT nanowire was aligned across adjacent electrodes (Fig. 1a) to serve as a positive template for shell deposition. The gap distance between electrodes was fixed at 3 μm. The entire assembly, including the electrodes and nanowire, was subsequently coated with ferromagnetic material by electrodeposition (Fig. 1b). All components of the completed structure are depicted in the cross-section drawing in Fig. 1c. SEM images of a completed device corresponding to the schematic in Fig. 1a are shown in Fig. 1d (45° tilt-view) and Fig. 1e (top-view). These images confirm that the PEDOT nanowire bridges the electrodes without contacting the underlying Si substrate, allowing for a complete ferromagnetic shell spanning from one electrode to the other. Because the electrodes are also coated with ferromagnetic material during fabrication, three different electrode shapes were investigated, including centered fingers, square, and rectangular. The different electrode shapes produced different aspect ratios and different magnetization directions measured relative to the nanowire axis. The centered finger electrodes had a high length to width ratio oriented with magnetization direction parallel to the nanowire, the rectangular electrodes had a low length to width ratio with magnetization direction oriented perpendicular to the nanowire, and the square electrodes had a length to width ratio of one with no preferred magnetization direction.

The tilt-view image in Fig. 1d illustrates that the core/shell nanowire is rigid (there is no apparent bending). Additionally there are solid contacts between the nanowire and the electrodes. By varying the deposition time, PEDOT/Ni nanowires with diameters of 500 nm, 600 nm, and 800 nm were synthesized. Assuming all of the PEDOT nanowires had a diameter of approximately 250 nm, the wall thicknesses of these shells were estimated to be approximately 125 nm, 175 nm, and 275 nm, respectively. These PEDOT/Ni nanowires had electrical resistances of 25 Ω, 15 Ω, and 6 Ω, respectively. The decrease in resistance with increasing diameter confirms that the larger diameters are due to greater shell thickness. A PEDOT/$Ni_{30}Fe_{30}$ core/shell nanowire with a shell thickness of approximately 150 nm was fabricated to investigate the influence of shell composition on MR behavior.

The TCR is defined as $\alpha = (\Delta R/R_{300\,K})(1/\Delta T)$, where $R_{300\,K}$ is the electrical resistance at 300 K and ΔR is the change in electrical resistance (i.e., $R_{(T)} - R_{300\,K}$) due to a temperature change of ΔT. The TCR was measured to identify the governing electrical transport mechanism in the core/shell nanowires. The resistance decreased with decreasing temperature, and the TCR values, shown in Fig. 2, are all positive, indicating metallic behavior. The TCR values range from 0.002 to 0.003, suggesting that electrical transport occurs predominately through the ferromagnetic shells [27]. The TCR values of the Ni/PEDOT core/shell nanowires had similar trends to those of Ni nanowires: for both, the TCR value decreased for decreasing characteristic dimension, i.e., wall thickness for the former and diameter for the latter. These results are expected, as smaller structures contain a larger fraction of surface atoms that scatter electrons nearly independent of temperature, which results in lower TCR values. In the case of core/shell nanowires, there is a comparatively large surface area fraction because there is both an interior and exterior surface.

The $\Delta R/R_O$ ratio is used to characterize the change in electrical resistance that occurs when the magnetic field is changed from zero field: $(\Delta R/R_O) = [R(H) - R(O)]/R(O)$. Here $R(O)$ is the electrical resistance of the core/shell nanowire in the absence of an applied magnetic field. In addition, $(\Delta R/R_O)_{//}$ denotes the longitudinal response, while $(\Delta R/R_O)_{\perp}$ denotes the transverse response. Fig. 3a and b show the dependence of the MR behavior on the magnetic field orientation for the 500 nm PEDOT/Ni nanowire measured at 300 K and 10 K, respectively. At 300 K, the electrical resistance of the PEDOT/Ni nanowire increased with decrease in the absolute value of the applied magnetic field from 50 kOe to 2 kOe. When the absolute value of the applied magnetic field was less than 2 kOe, the electrical resistance decreased with decrease in absolute value

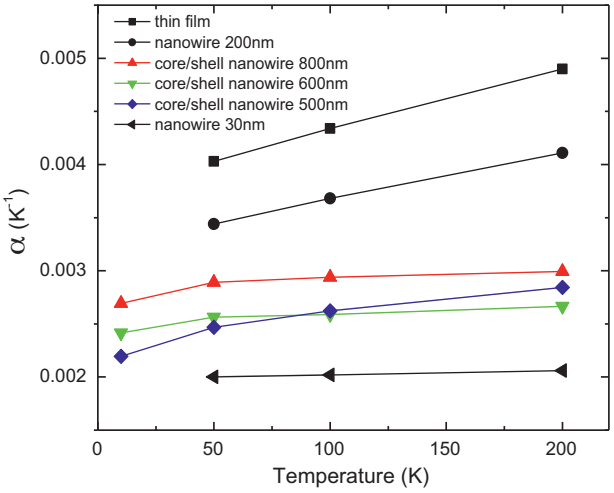

Fig. 2. Temperature dependent coefficient of resistance (TCR) for Ni thin films, solid Ni nanowires [27], and PEDOT/Ni core/shell nanowires.

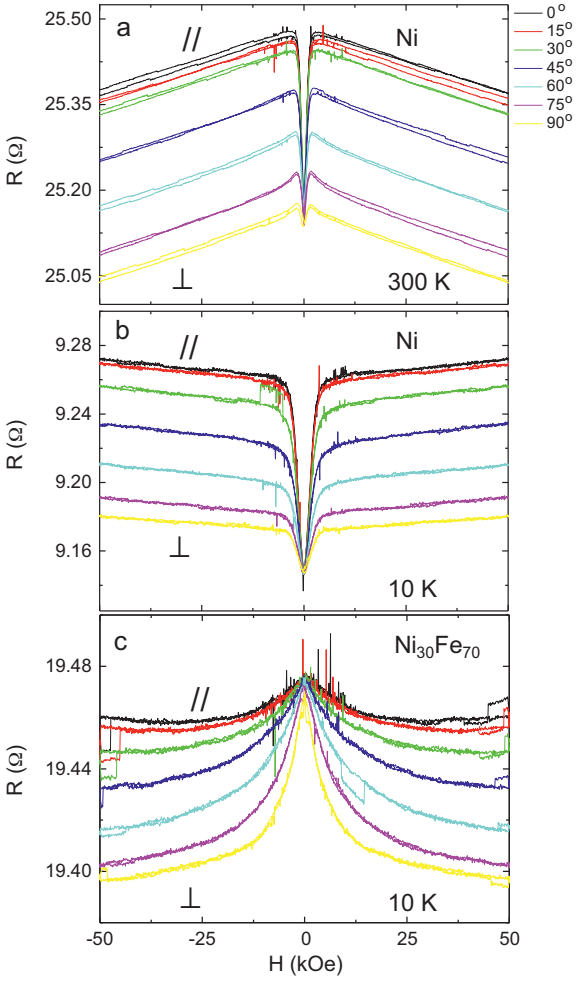

Fig. 3. Typical orientation dependent magnetoresistance of single PEDOT/Ni core/shell nanowire measured at 300 K (a) and 10 K (b) and single PEDOT/$Ni_{30}Fe_{70}$ core/shell nanowire at 10 K (c). (//: longitudinal direction, ⊥: transverse direction).

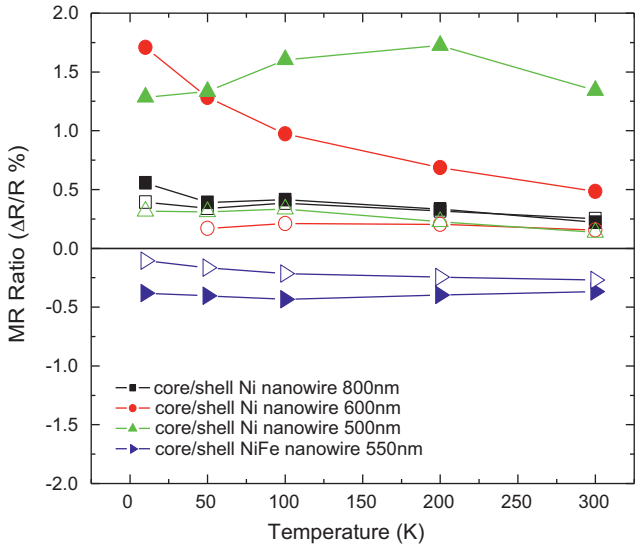

Fig. 4. Temperature dependent MR behavior for PEDOT/Ni and PEDOT/$Ni_{30}Fe_{70}$ nanowires. Filled and open symbols represent longitudinal and transverse $\Delta R/R_o$, respectively.

of applied magnetic field (Fig. 3a). At 10 K, the electrical resistance of the PEDOT/Ni nanowire monotonically decreased with decrease in the absolute value of the applied magnetic field (Fig. 3b). Thus, at low applied magnetic field (i.e., $|H| < 2$ kOe) for both 300 K and 10 K, the PEDOT/Ni nanowire displayed positive $\Delta R/R_O$ values independent of the magnetic field orientation. The $(\Delta R/R_O)_{//}$ ratios of PEDOT/Ni nanowires were consistent with characteristic positive AMR behavior in Ni nanowires and thin films, while the $(\Delta R/R_O)_{\perp}$ ratios were all opposite in sign to negative AMR values. Surprisingly, the PEDOT/$Ni_{30}Fe_{70}$ core/shell nanowire had MR behavior different from that of a PEDOT/Ni nanowire, with negative $\Delta R/R_O$ ratio for both orientations and a maximum $\Delta R/R_O$ ratio in the transverse direction (Fig. 3c).

The temperature-dependent magnetoresistance of PEDOT/Ni and PEDOT/$Ni_{30}Fe_{70}$ core/shell nanowires is illustrated in Fig. 4. Both $(\Delta R/R_O)_{//}$ and $(\Delta R/R_O)_{\perp}$ of PEDOT/Ni nanowires are positive and significantly different from that of solid Ni nanowires, which display typical AMR behavior with positive $(\Delta R/R_O)_{//}$ and negative $(\Delta R/R_O)_{\perp}$ ratios [27]. In addition, the magnitude of $(\Delta R/R_O)_{\perp}$ for core/shell nanowires displays a weak dependence on shell thickness and temperature, deviating from the clear increase in the magnitude of $(\Delta R/R_O)_{\perp}$ with decreasing diameter for solid Ni nanowires. However, the most resistive PEDOT/Ni core/shell nanowire (i.e., 25 Ω for 500 nm PEDOT/Ni core/shell nanowire with shell thickness of approx. 125 nm) exhibits $(\Delta R/R_O)_{//}$ similar to that of a 200 nm solid nickel nanowire with maximum $(\Delta R/R_O)_{//}$ ratio at around 200 K. Conversely, larger and more conductive core/shell nanowires (i.e., 600 nm and 800 nm PEDOT/Ni core/shell nanowires) displayed monotonically decreasing $(\Delta R/R_O)_{//}$ ratio with increasing temperature.

Although the exact mechanism of MR behavior of core/shell nanowires is difficult to ascertain due to the complexity of the device, systematic experiments were conducted to gain insights. To investigate the effect of spin constriction between the electrode and ferromagnetic shell, PEDOT/Ni core/shell nanowires were fabricated on electrodes with different shapes (i.e., square, rectangular, and centered fingers with different length to width ratios). The MR behavior of PEDOT/Ni core/shell nanowires was independent of electrode shape, which indicates that spin constriction between the electrode and ferromagnetic shell does not play an important role.

Unique MR behaviors reported herein may be attributed to a magnetostriction induced response. Unlike solid nanowires, the soft and flexible polymer core may permit expansion and contraction of the shell similar to a hollow ferromagnetic tube. Because Ni has a positive transverse saturation magnetostriction of $\sim 20 \times 10^{-6}\ \Delta l/l$, the shell length increases with increasing applied magnetic field strength, and accordingly the cross-sectional area decreases as Ni has a negligible volume magnetostriction of $-0.06 \times 10^{-6}\ \Delta v/v$ [28]. A decreased cross-sectional area would cause an increase in electrical resistance under applied magnetic fields and is therefore consistent with the observed positive values of $(\Delta R/R_O)_{\perp}$ in the PEDOT/Ni core/shell nanowires. In addition, it has been reported that magnetostriction of bulk Ni reaches its saturation value around 2kOe at room temperature, similar to the PEDOT/Ni MR behaviors in Fig. 3b. Additionally, the saturation magnetostriction of bulk nickel increases nearly three fold as the temperature is reduced from 300 K to 10 K, which is similar to the increase in $(\Delta R/R_O)_{\perp}$ in our work [28]. Magnetostriction hysteresis is also consistent with the magneto-transport hysteresis of PEDOT/Ni core/shell nanowires [29]. Furthermore, the large positive volume magnetostriction of $Ni_{30}Fe_{70}$ ($>35 \times 10^{-6}\ \Delta v/v$) [30], which is over two orders of magnitude greater (in absolute value) than the negative volume magnetostriction for Ni, may explain the negative values of $(\Delta R/R_O)_{//}$ and $(\Delta R/R_O)_{\perp}$ since the volume magnetostriction leads to an overall decrease in resistance regardless of the orientation due to the increase in cross-sectional area of the shell. Although the values of $(\Delta R/R_O)_{//}$ and $(\Delta R/R_O)_{\perp}$ of both Ni and $Ni_{30}Fe_{70}$ core/shell nanowires followed the magnetostriction trends, the MR behaviors cannot be explained solely by magnetostriction because the expected resistance changes of a ferromagnetic shell due to magnetostriction is two or three orders of magnitude lower than the observed values of $\Delta R/R_O$.

Domain formation within the tubular geometry of the ferromagnetic shell may play a critical role in the magneto-transport properties because it eliminates a mathematical singularity found in wires. In the absence of an applied magnetic field, ferromagnetic shells with inner radius to outer radius ratios of 0.25–0.4 and lengths of 3 μm exhibit vortex magnetization in which the shell is circularly magnetized around its annular cross-section (Fig. 5a) [9,11,31,32]. For shorter and thicker shells, this magnetization state becomes more stable such that there are fewer domains than for longer and thinner shells. In contrast, high applied magnetic fields in the longitudinal direction yield a magnetization state parallel to the nanowire axis which induces transverse domain walls at the ends of the core/shell nanowire and along the axial length (Fig. 5b). The domain wall density is dependent upon several factors (shell thickness, defect sites, length to shell ratio, etc.) but the domain walls at the shell/electrode interface are believed to be more severe due the abrupt change in both cross-section and geometry. Therefore, if the vortex state minimizes domain wall formation and domain walls act as scattering sites, electrical resistance will increase with increased applied magnetic field parallel to the nanowire axis. Thus, the trend of $(\Delta R/R_O)_{//}$ in PEDOT/Ni nanowires may be a combination of positive longitudinal AMR and positive domain wall magnetoresistance.

A high transverse magnetic field direction is expected to create an onion magnetization with transverse domain walls aligned parallel to both the field and nanowire axis, splitting the ferromagnetic shell down the middle into two domains (Fig. 5c). Domain splitting might extend along the entire length of the shell, behaving as a high resistance pathway whose impact may be compounded by the Hall voltage between the two shell halves, ultimately decreasing the carrier mean free path and increasing electrical resistance. Thus $(\Delta R/R_O)_{\perp}$ response is also a combination of geometry induced MR and AMR where geometrically induced MR in the transverse direction is greater than in the

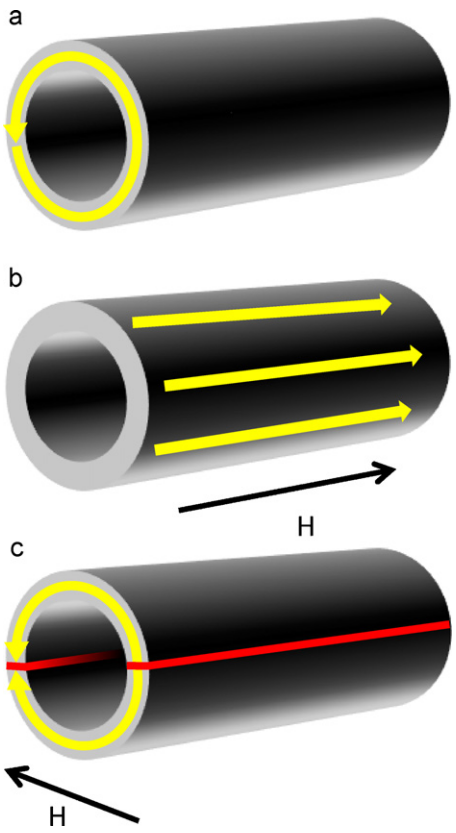

Fig. 5. Schematic representation of magnetization states of ferromagnetic shells: (a) in the absence of applied magnetic field and in the presence of applied magnetic field in the (b) longitudinal and (c) transverse direction of the tube axis. The red lines represent domain walls and the yellow arrows indicate the magnetization. (For interpretation of the references to color in this figure legend, the reader is referred to the web version of the article.)

longitudinal direction. Domain wall effects can easily be on the order of one percent with reported domain wall magnetoresistance of 1.7% for Ni and −0.1% for $Ni_{30}Fe_{70}$. However, the actual value of $\Delta R/R$ is highly dependent on the exact domain configuration and wall thickness [33,34]. Although the influence of each mechanism on the overall MR behavior is difficult to quantify without observing magnetic domain formation, evaluation of magnetostriction and magnetization states suggest domain wall magnetoresistance (DWMR) may play an important role in these core/shell nanowires. The MR behavior of conducting polymer core/ferromagnetic shell nanowires is also consistent with the experimental results from a Ni-rich permalloy nanoconstriction [35].

4. Conclusions

In summary, single PEDOT/ferromagnetic core/shell nanowires were fabricated by electrodeposition of ferromagnetic materials (Ni and $Ni_{30}Fe_{70}$) on PEDOT nanowire assemblies. The shape and material of the prefabricated electrodes were varied to discount their influence. The TCR of PEDOT/Ni core/shell nanowires followed a similar trend to that of solid Ni nanowires, indicating electrons were predominately transported though the ferromagnetic shell. The MR behaviors of PEDOT/Ni and PEDOT/$Ni_{30}Fe_{70}$ core/shell nanowires behaved differently than their solid nanowire counterparts. The anomalous MR behavior was attributed to geometry induced MR transpiring from domain wall formation within the ferromagnetic shell. Further investigation of magneto-transport properties and configurations of domain walls are required to support future developments in magnetic sensors, spintronics, and magnetic random access memory.

Acknowledgment

This material is based on research sponsored by the Defense Microelectronics Activity (DMEA) under agreement number DOD/DMEA-CNN H94003-06-20604. The United States government is authorized to reproduce and distribute reprints for government purposes, not withstanding any copyright notation thereon.

References

[1] S. Khizroev, M.H. Kryder, D. Litvinov, D.A. Thompson, Appl. Phys. Lett. 81 (2002) 2256.
[2] S. Son, J. Reichel, B. He, M. Schuchman, S. Lee, J. Am. Chem. Soc. 127 (2005) 7316.
[3] J. Xie, L. Chen, V. Varadan, J. Yancey, M. Srivatsan, Nanotechnology 19 (2008) 105101.
[4] J. Joo, B. Kim, D. Park, H. Kim, D. Seo, J. Shim, S. Lee, K. Ryu, K. Kim, J. Jin, T. Lee, C. Lee, Synth. Met. 153 (2005) 313.
[5] J. Joo, D.H. Park, M.Y. Jeong, Y.B. Lee, H.S. Kim, W.J. Choi, Q.H. Park, H.J. Kim, D.C. Kim, J. Kim, Adv. Mater. 19 (2007) 2824.
[6] D.H. Park, M.Y. Jeong, M. Kim, E.H. Cho, D.C. Kim, H. Song, J. Kim, T.K. Shim, D. Kim, J. Joo, J. Nanosci. Nanotechnol. 9 (2009) 3112.
[7] D.H. Park, H.S. Kim, M.Y. Jeong, Y.B. Lee, H.J. Kim, D.C. Kim, J. Kim, J. Joo, Adv. Funct. Mater. 18 (2008) 2526.
[8] J. Bachmann, J. Escrig, K. Pitzschel, J. Moreno, J. Jing, D. Gorlitz, D. Altbir, K. Nielsch, J. Appl. Phys. 105 (7) (2009) B521.
[9] J. Escrig, P. Landeros, D. Altbir, E. Vogel, J. Magn. Magn. Mater. 310 (2007) 2448.
[10] P. Landeros, S. Allende, J. Escrig, E. Salcedo, D. Altbir, E. Vogel, Appl. Phys. Lett. 90 (2007) 102501.
[11] P. Landeros, O. Suarez, A. Cuchillo, P. Vargas, Phys. Rev. B 79 (2009) 024404.
[12] Z. Wang, H. Lim, H. Liu, S. Ng, M. Kuok, L. Tay, D. Lockwood, M. Cottam, K. Hobbs, P. Larson, J. Keay, G. Lian, M. Johnson, Phys. Rev. Lett. 94 (2005) 137208.
[13] X. Han, S. Shamaila, R. Sharif, J. Chen, H. Liu, D. Liu, Adv. Mater. 21 (2009) 4619.
[14] F. Tao, M. Guan, Y. Jiang, J. Zhu, Z. Xu, Z. Xue, Adv. Mater. 18 (2006) 2161.
[15] L. Liu, W. Zhou, S. Xie, L. Song, S. Luo, D. Liu, J. Shen, Z. Zhang, Y. Xiang, W. Ma, Y. Ren, C. Wang, G. Wang, J. Phys. Chem. C 112 (2008) 2256.
[16] Y. Sui, R. Skomski, K. Sorge, D. Sellmyer, J. Appl. Phys. 95 (2004) 7151.
[17] Y. Sui, R. Skomski, K. Sorge, D. Sellmyer, Appl. Phys. Lett. 84 (2004) 1525.
[18] M. Daub, M. Knez, U. Goesele, K. Nielsch, J. Appl. Phys. 101 (9) (2007) J111.
[19] K. Pitzschel, J. Moreno, J. Escrig, O. Albrecht, K. Nielsch, J. Bachmann, ACS Nano 3 (2009) 3463.
[20] Q. Wang, B. Geng, S. Wang, Y. Ye, B. Tao, Chem. Commun. 46 (2010) 1899.
[21] Z. Liu, D. Zhang, S. Han, C. Li, B. Lei, W. Lu, J. Fang, C. Zhou, J. Am. Chem. Soc. 127 (2005) 6.
[22] J. Curiale, R. Sachez, H. Troiani, C. Ramos, H. Pastoriza, A. Leyva, P. Levy, Phys. Rev. B 75 (2007) 224410.
[23] S.A. Solin, T. Thio, D.R. Hines, J.J. Heremans, Science 289 (2000) 1530.
[24] J. Lee, J. Hong, K. Rhie, S. Ahn, J. Kim, J. Lee, K.H. Shin, B.C. Lee, Phys. Status Solidi A – Appl. Res. 201 (2004) 1965.
[25] K. Nielsch, F. Castano, S. Matthias, W. Lee, C. Ross, Adv. Eng. Mater. 7 (2005) 217.
[26] K. Nielsch, F. Castano, C. Ross, R. Krishnan, J. Appl. Phys. 98 (2005) 034318.
[27] Y. Rheem, B.Y. Yoo, W.P. Beyermann, N.V. Myung, Nanotechnology 18 (2007) 015202.
[28] R.M. Bozorth, Ferromagnetism, IEEE Press, Piscataway, NJ, 1993.
[29] K. Sekiguchi, E. Saitoh, H. Miyajima, J. Appl. Phys. 97 (2005).
[30] Y. Tino, T. Maeda, J. Phys. Soc. Jpn. 24 (1968) 729.
[31] M. Steiner, J. Nitta, Appl. Phys. Lett. 84 (2004) 939.
[32] F. Zhu, G. Chern, O. Tchernyshyov, X. Zhu, J. Zhu, C. Chien, Phys. Rev. Lett. 96 (2006) 027205.
[33] S. Lepadatu, Y.B. Xu, Phys. Rev. Lett. 92 (2004).
[34] U. Ruediger, J. Yu, S. Zhang, A. Kent, S. Parkin, Phys. Rev. Lett. 80 (1998) 5639.
[35] R. van Gorkom, J. Caro, S. Theeuwen, K. Wellock, N. Gribov, S. Radelaar, Appl. Phys. Lett. 74 (1999) 422.